J Mater Sci: Mater Med (2013) 24:2371–2379
DOI 10.1007/s10856-013-4993-3

Transferrin-conjugated, fluorescein-loaded magnetic nanoparticles for targeted delivery across the blood–brain barrier

Feng Yan · Ying Wang · Shenzhi He · Shuting Ku · Wei Gu · Ling Ye

Received: 28 January 2013 / Accepted: 15 June 2013 / Published online: 23 June 2013

Abstract The blood–brain barrier (BBB) restricts the delivery of many potentially important therapeutic agents for the treatment of brain disorders. An efficient strategy for brain targeted delivery is the utilization of the targeting ligand conjugated nanoparticles to trigger the receptor-mediated transcytosis. In this study, transferrin (Tf) was employed as a brain targeting ligand to functionalize the fluorescein-loaded magnetic nanoparticles (FMNs). The Tf conjugated FMNs (Tf-FMNs) were characterized by transmission electron microscopy, thermal gravimetric analysis, Fourier transform infrared spectroscopy, and X-ray photoelectron spectroscopy. Using fluorescein as an optical probe, the potential of Tf-FMNs as brain targeting drug carriers was explored in vivo. It was demonstrated that Tf-FMNs were able to cross the intact BBB, diffuse into brain neurons, and distribute in the cytoplasm, dendrites, axons, and synapses of neurons. In contrast, magnetic nanoparticles without Tf conjugation cannot cross the BBB efficiently under the same conditions. Therefore, Tf-FMNs hold great potential in serving as an efficient multifunctional platform for the brain-targeted theranostics.

Feng Yan and Ying Wang have contributed equally to this work.

F. Yan
Xuanwu Hospital, Capital Medical University, Beijing 100053, People's Republic of China

Y. Wang
Department of Laboratory Animal, Capital Medical University, Beijing 100069, People's Republic of China

S. He · S. Ku · W. Gu (✉) · L. Ye (✉)
School of Chemical Biology and Pharmaceutical Sciences, Capital Medical University, Beijing 100069, People's Republic of China
e-mail: weigu@ccmu.edu.cn

L. Ye
e-mail: lingye@ccmu.edu.cn

1 Introduction

Nanoparticles based drug carriers for cancer targeting and therapy have become the most productive area in biomedical research field. As drug carriers, nanoparticles could protect drug against degradation and premature release and reduce side effects. Compared with other nanoparticles, superparamagnetic Fe_3O_4 nanoparticles exhibit higher biocompatibility and chemical stability. Furthermore, nontoxic materials, such as silica or polymer, can be easily coated onto magnetic nanoparticles for surface modification with amino or carboxyl groups, which can be further conjugated with another functional biomolecules. Fe_3O_4 nanoparticles have shown great potentials in acting as carriers for the targeted drug delivery [1, 2]. However, Fe_3O_4-based drug delivery system may suffer from the inability to cross biological barriers, especially the blood–brain barrier (BBB).

The BBB is a dynamic interface between the blood and the brain formed by brain capillary endothelial cells sealed with continuous tight junctions to protect the brain from invasion of various circulating toxins and other harmful molecules. With very few exceptions, only lipophilic and low molecular weight molecules can passively cross the BBB. On the other hand, the BBB, however, represents one of the most exclusive biological barriers encountered in the treatment of neurological diseases, restricting the access of most diagnosis and therapeutic agents to the brain via the systemic route [3, 4]. Therefore, the challenge in treating most brain disorders is to overcome the difficulty of delivering therapeutic agents to targeted regions of the

brain by crossing the BBB. Fortunately, brain capillary endothelia cells show some specific receptor-mediated transport mechanisms. It has been documented that a high level of transferrin receptor (TfR) is expressed by brain capillary endothelia cells involved in receptor-mediated transcytosis through the BBB [5, 6]. These receptors can be targeted with corresponding ligands. As a result, transferrin (Tf) is allowed free access across the intact BBB and functions as carrier of essential nutrients into the brain. Inspired by this, Tf is applied as an attractive targeting ligand to functionalize the nanoparticles in order to selectively bind BBB endothelium and triggers the receptor-mediated transcytosis of nanoparticles across the BBB. This receptor-mediated delivery system is becoming one of the most promising non-invasive approaches to overcome the BBB. The receptor-mediated transport of liposomal and polymeric nanoparticulate formulations across the intact BBB has been demonstrated. Nevertheless, using biocompatible inorganic nanoparticles which are structurally robust and capable to transporting multiple agents to actively cross the BBB is highly desirable.

Herein, we first synthesized magnetic Fe_3O_4 nanoparticles covered with mesoporous silica shell, which serves as an insulator and allow the encapsulation of the fluorescein (FITC) as an optical probe. The BBB targeting ligand Tf was then conjugated onto those FITC-loaded magnetic nanoparticles (FMNs) via the polyethylene glycol (PEG_{5k}) linker. The integration of PEG chains provides a steric stabilizing layer, which prevents the aggregation of nanoparticles under the physiologic conditions and consequently reduce protein adsorption. Moreover, amphiphilic PEG with high lipid solubility may increase the endothelial permeability [7], and thus facilitate the BBB passage in line with Tf. Such Tf conjugated nanocarrier therefore is expected to be able to overcome the BBB and delivery to specific brain regions. To verify the BBB crossing ability provided by Tf conjugation, the rat brain was sliced and examined by confocal laser scanning microscope (CLSM) and transmission electron microscopy (TEM) after administration of Tf-FMNs. In addition, the brain distribution of Tf-FMNs was explored as well.

2 Materials and methods

2.1 Materials and animals

Fluorescein isothiocyanate isomer I (FITC), 3-aminopropyltriethoxysilane (APTES), holo-transferrin (Tf) human ≥97 %, 4′,6-diamidino-2-phenyindole (DAPI), mouse anti-NeuN antibody, Alexa 594-conjugated goat anti-mouse IgG and 5,5′-dithiobis-(2-nitrobenzoic acid) (Ellman's reagent) were purchased from Sigma-Aldrich (USA). 3-mercaptopropyltrimethoxysilane (MPTMS, 95 %) was purchased from Alfa Aesar. The Micro BCA protein assay kit was purchased from Pierce. NHS-PEG_{5k}-Mal was purchased from Jenkem Technology CO. Ltd. (Beijing, China). All other reagents were of analytical grade and used as received.

Male Wistar rats with body weight of 260–280 g were purchased from the Department of laboratory animals, Capital Medical University (China) and maintained under standard housing conditions. All animal experiments were treated according to protocols evaluated and approved by the ethical committee of Capital Medical University.

2.2 Synthesis

Magnetic Fe_3O_4 nanoparticles were synthesized according to procedure reported in the literatures [8, 9]. To obtain FMNs, 40 mg of Fe_3O_4 nanoparticles, 308 ml of cyclohexane, 75.5 ml of Triton X-100, 64 ml of hexylalcohol, and 13.6 ml of H_2O were mixed to generate a microemulsion for 30 min, followed by the addition of 1.6 ml of tetraethoxysilane (TEOS). After stirring for 6 h, 4.64 ml of aqueous ammonia (25 wt%) was introduced dropwise to initiate the hydrolysis, and the microemulsion was kept stirring for 24 h. Finally, to the above microemulsion, 0.8 ml of FITC-APTES (FITC-APTES was prepared by mixing 4.2 mg of FITC with 58.6 μl of APTES in 0.8 ml of absolute ethanol for 24 h in room temperature) and 1.2 ml of TEOS were added, followed by stirring for 24 h. After the reaction was complete, the resulting FMNs were isolated by magnetic separation, washed five times with anhydrous ethanol, and dispersed in anhydrous ethanol.

The synthesis of FMN-SH was conducted by dispersing 100 mg of FMNs in 40 ml of absolute ethanol, followed by the addition of 0.2 ml of MPTMS. The suspension was heated to 78 °C and refluxed at this temperature for 6 h [10]. The resulting mixture was then isolated with an Nd–Fe–B magnet and washed with 95 % ethanol and sterile saline twice. The obtained FMN-SH was stored in sterile saline at 4 °C. The surface thiol group was assayed to be 55 μmol thiol groups per gram FMN-SH via Ellman's reagent.

Tf-PEG_{5k}-Mal was prepared according to the previously reported protocol [10]. First, Tf (50 mg) was reacted with NHS-PEG_{5k}-Mal (75 mg) in 300 ml of PBS (100 mM, pH 8) for 2 h at 20 °C. The unconjugated NHS-PEG_{5k}-Mal was removed centrifugally by a spin column with a membrane pore size of 10 kDa at 6000 g for 15 min. The resulting Tf-PEG_{5k}-Mal was washed with sterile saline (pH 7.4) three times. Next, 100 mg of FMN-SH were mixed with 100 mg of Tf-PEG-Mal in 300 ml of PBS at pH 7.4. The above mixture was then cooled down to 4 °C and kept slowly stirring for 24 h. The obtained Tf-FMNs was

collected by magnetic separation, washed with sterile saline four times, and stored in sterile saline at 4 °C. The Tf conjugation is about 905 ng per mg Tf-FMNs as evaluated by bicinchoninic acid (BCA) protein assay kit.

2.3 Characterizations

The Tf-FMNs were characterized by TEM, thermal gravimetric analysis (TGA), Fourier transform infrared spectroscopy (FTIR), X-ray diffraction (XRD), and X-ray photoelectron spectroscopy (XPS). XRD was performed on a Rigaku SmartLab X-ray diffractometer (Cu K_α radiation $\lambda = 1.54056$ Å). TEM (JEM-2010, JEOL, Japan) was used to observe the sizes and the morphologies of both FMNs and Tf-FMNs. For TEM imaging, a drop of nanoparticle dispersed in ethanol was placed on a carbon-coated copper grid and dried in a vacuum desiccator. TGA and DTG curves were collected on a TGA Q50 V20.6 instrument with a heating rate of 10 °C min^{-1} under nitrogen atmosphere. FTIR spectra were recorded on a NICOLET AVATAR 300 spectrometer. Typically, sample powder (1 mg) was mixed with KBr (99 mg) and pressed into pellet with minimum pressure. XPS were performed to analyze the surface composition of nanoparticles on a PHI 5300 ESCA System (Perkin Elmer) at 250 W (12.5 kV and 20 mA) under an ultravacuum of 10^{-6} Pa (10^{-8} Torr) using the Mg Kα line.

2.4 Animal experiment

Male Wistar rats (260–280 g) were anesthetized with an i.p. injection of 10 % chloral hydrate (1.2 ml/kg). A midline incision was made on the neck and two branches of external carotid artery (ECA) were cut by electro coagulation. After the ECA was ligated in front of the occipital artery branch, the distal portion of the ligation site was immediately electro-coagulated. FMNs or Tf-FMNs in physiological saline (2 ml) were perfused into the internal carotid artery (ICA) using an infusion pump (2 mg/2 ml/280 g), and this was followed by 0.5 ml of simil–plasma fluid. After this, the proximal portion of the ECA was ligated and the wound was finely sutured [11]. One hour later, rats were sacrificed by heart perfusion of physiological saline, followed by 4 % paraformaldehyde. Then various organs (brain, heart, liver, spleen, lung and kidney) were collected and washed with distilled water for further analysis.

2.5 Confocal laser scanning microscope (CLSM)

The organs were fixed in 4 % paraformaldehyde solution and dehydrated in 30 % sucrose solution for approximately 48 h, then sectioned on a cryostat with a 30 μm thickness. Sections were fixed on a glass slide and cell nuclei were stained with DAPI (1 μg/ml) and subsequently mounted with 75 % glycerol in PBS (0.01 M, pH 8). Imaging was performed on a CLSM (SP5 LAS AF, Leica).

2.6 Transmission electron microscopy (TEM)

The brains were post-fixed in 2.5 % glutaraldehyde solution and 1 % osmium tetroxide, dehydrated in increasing ethanol concentrations and subsequently embedded in the epoxy resin. The embedded tissues were cut into ultra-thin sections with an ultramicrotome and mounted on general copper grids. After being stained with uranyl acetate and lead citrate, the specimens were observed with TEM (HITACHI-7650).

2.7 Immunofluorescence staining

The brains were fixed in 4 % paraformaldehyde solution and dehydrated in 30 % sucrose solution for approximately 48 h, and then sectioned on a cryostat at 50 μm thickness for immunofluorescence staining. The brain sections were first incubated with mouse anti-NeuN antibody (1:1,000 in 0.01 M PBST) for 24 h. Next, the sections were incubated with Alexa594-conjugated goat anti-mouse IgG (1:300, in 0.01 M PBST) in the dark for 2–3 h. Finally, the sections were mounted with 75 % glycerol and observed using the CLSM (SP5 LAS AF, Leica) with dual excitation band of Alexa 594 and FITC using an emission filter set.

3 Results and discussion

To obtain Tf-FMNs, Fe_3O_4 nanoparticles were first synthesized, followed by coated with a mesoporous silica shell, functionalized with thiol groups, and then conjugated with Tf through the bifunctional PEG (NHS-PEG_{5k}-Mal). Although this study focused on the effect of Tf conjugation on the BBB penetration of FMNs, it is noteworthy that the mesoporous silica shell could be used for encapsulation and controlled release of therapeutic agents [12–15]. Moreover, by encapsulating therapeutic agents in the silica shell, the surface properties of Tf-FMNs remain unchanged. Therefore, the perturbation of BBB penetration due to the drug loading could be ignored.

Figure 1 showed the XRD patterns of the FMNs and Tf-FMNs. The patterns of the FMNs can be readily indexed to pure Fe_3O_4 with the cubic inverse spinel structure. Specifically, the main diffractions appeared at $2\theta = 35.4°$, 56.7° and 62.74°, which could be primarily attributed to the (331), (511) and (440) planes of Fe_3O_4, respectively. The diffraction pattern of Tf-FMNs were similar to that of FMNs, and no extra peaks were observed, implying that the

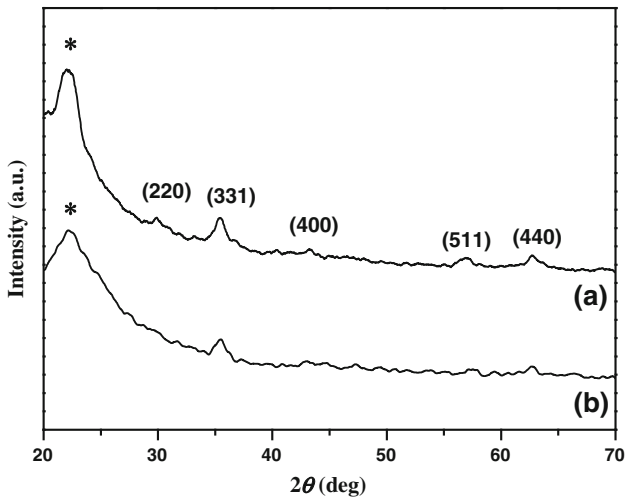

Fig. 1 XRD patterns of (*a*) FMNs and (*b*) Tf-FMNs. * is due to amorphous silica

crystalline structure of the FMNs was well maintained upon Tf conjugation [16].

The sizes and morphologies of FMNs and Tf-FMNs were examined by TEM. As shown in Fig. 2, the sphere-shaped morphology of FMN with a diameter of about 80–90 nm and a slight increase in diameter was observed after Tf conjugation.

The conjugation of Tf onto FMNs was first confirmed by the TGA. The obtained TGA curves are presented in Fig. 3. Obviously, the weight loss of FMNs could be categorized into two segments. The first weight loss below 460 °C were probably due to the desorption of ethanol and water, respectively. The following weight loss in the temperature range of 460–660 °C corresponded to the decomposition of FTIC and APTES. No further weight loss occurred with the increase of temperature and the total weight loss of the FMNs was about 17 %. The same weight loss was also found in the TGA plot of Tf-FMNs below 660 °C. However, increasing of the temperature led to an additional

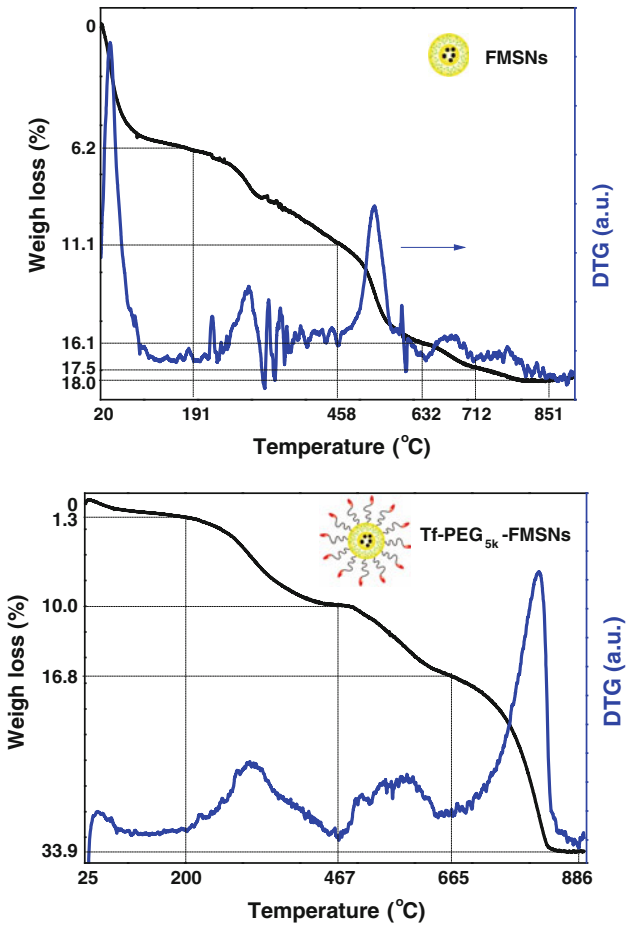

Fig. 3 TGA and DTG curves of FMNs and Tf-FMNs (Color figure online)

weigh loss of 18 %, which most likely resulted from the desorption of conjugated Tf-PEG_{5k}. It should be noted that the increase in desorption temperature for Tf-PEG5 k is indicative of an increased bonding strength to the FMNs' surface due to the covalent nature of the MPTMS silane linkage [17].

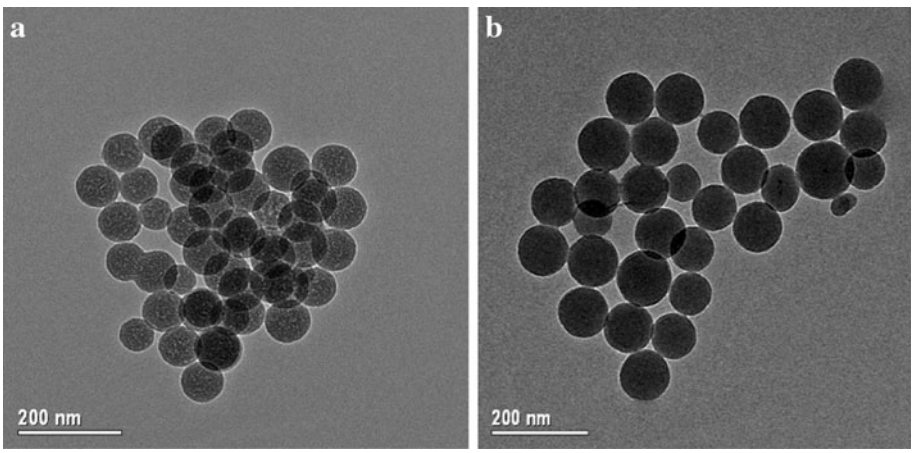

Fig. 2 TEM images of **a** FMNs and **b** Tf-FMNs

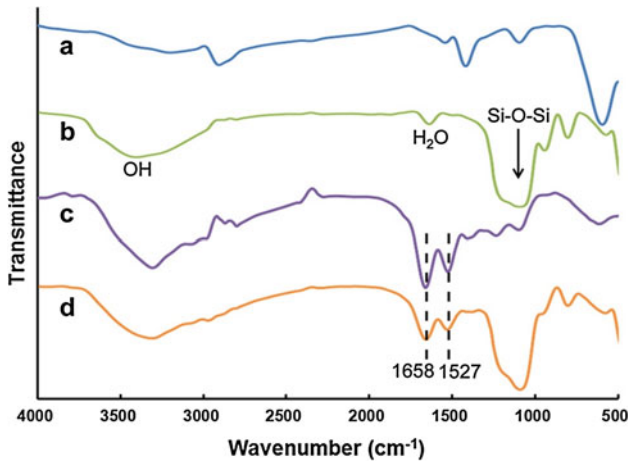

Fig. 4 FTIR spectra of *a* Fe_3O_4 nanoparticles, *b* FMNs, *c* Tf, and *d* Tf-FMSNs (Color figure online)

FTIR spectroscopic studies further verified the Tf conjugation. Compared to the IR spectrum of Fe_3O_4 (Fig. 4a), two new IR bands at 1,080 and 3,300 cm^{-1} were observed in the IR spectrum of FMNs (Fig. 4b). These two bands can be respectively attributed to the stretching mode of Si–O–Si and hydrogen-bonded silanol, suggesting that the silica shell was formed over the Fe_3O_4 core. The IR spectrum of the Tf (Fig. 4c) showed the amide I and amide II bands at 1,658 and 1,527 cm^{-1}, respectively. These characteristic amide bands were also presented in the IR spectrum of Tf-FMNs (Fig. 5d), indicating the successful conjugation of Tf onto FMNs.

Moreover, the XPS was used to explore the change of the surface elemental compositions of FMNs upon Tf conjugation. XPS is highly surface specific and is very useful for the detection of surface elemental information of particles. The surface atomic ratios calculated from the XPS are listed in Table 1. The Si content of FMNs was 32.6 %, which decreased sharply to 11.5 % for Tf-FMNs. Correspondingly, the surface atomic ratios of Fe/Si, N/Si and C/Si all increased upon the conjugation of PEG-Tf, and especially the atomic ratio of Fe/Si of Tf-FMNs was about six times higher than that of FMNs. Therefore, the XPS results together with TGA and FTIR strongly suggested the successful conjugation of Tf on the FMNs.

Table 1 Surface elemental contents of Si and atomic ratios of Fe/Si, N/Si, and C/Si calculated from the corresponding XPS

	Si/%	Fe/Si	N/Si	C/Si
FMNs	32.6	0.3	0.1	0.9
Tf-FMNs	11.5	1.6	0.7	3.1

Next, the biodistribution of FMNs with or without Tf conjugation was investigated. The sections (30 μm) of brain, heart, liver, spleen, lung and kidney were stained with DAPI (a nucleus-staining blue fluorescent dye) and then were examined immediately by CLSM. As displayed in Fig. 5, FMNs (Fig. 5a–e) and Tf-FMNs (Fig. 5f–j) with a green fluorescence signal originating from the labelled FITC were observed not only in spleen, lung and liver, but in heart, kidney, and more important, in brain (Fig. 6). In comparison with the abundant accumulation of FMNs (Fig. 5b, d), Tf-FMNs showed a reduced uptake in liver and lung (Fig. 5g, i), implying that Tf-FMNs had a longer half-life than that of bare FMNs [18]. This could be attributed to the PEG chains that protect nanoparticles from binding of serum proteins and degradation. The reduced accumulation in the lung and liver might minimize the acute adverse effects such as breathing problems or liver necrosis when Tf-FMNs were administered.

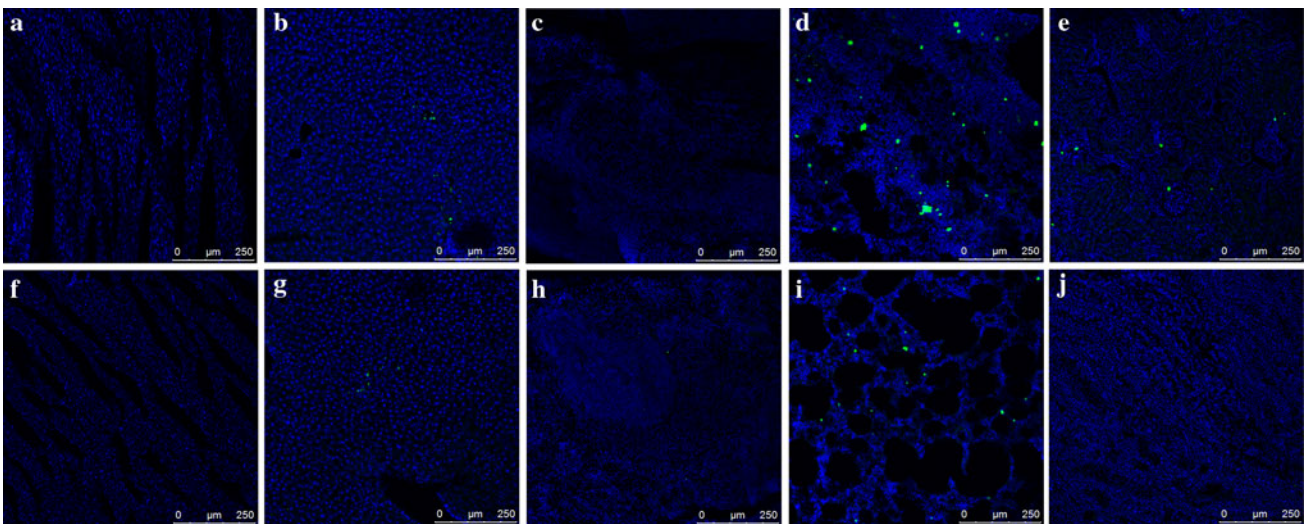

Fig. 5 The distribution of FMNs (**a**–**e**) and Tf-FMNs (**f**–**j**) in heart (**a**, **f**), liver (**b**, **g**), spleen (**c**, **h**), lung (**d**, **i**), kidney (**e**, **j**) (Color figure online)

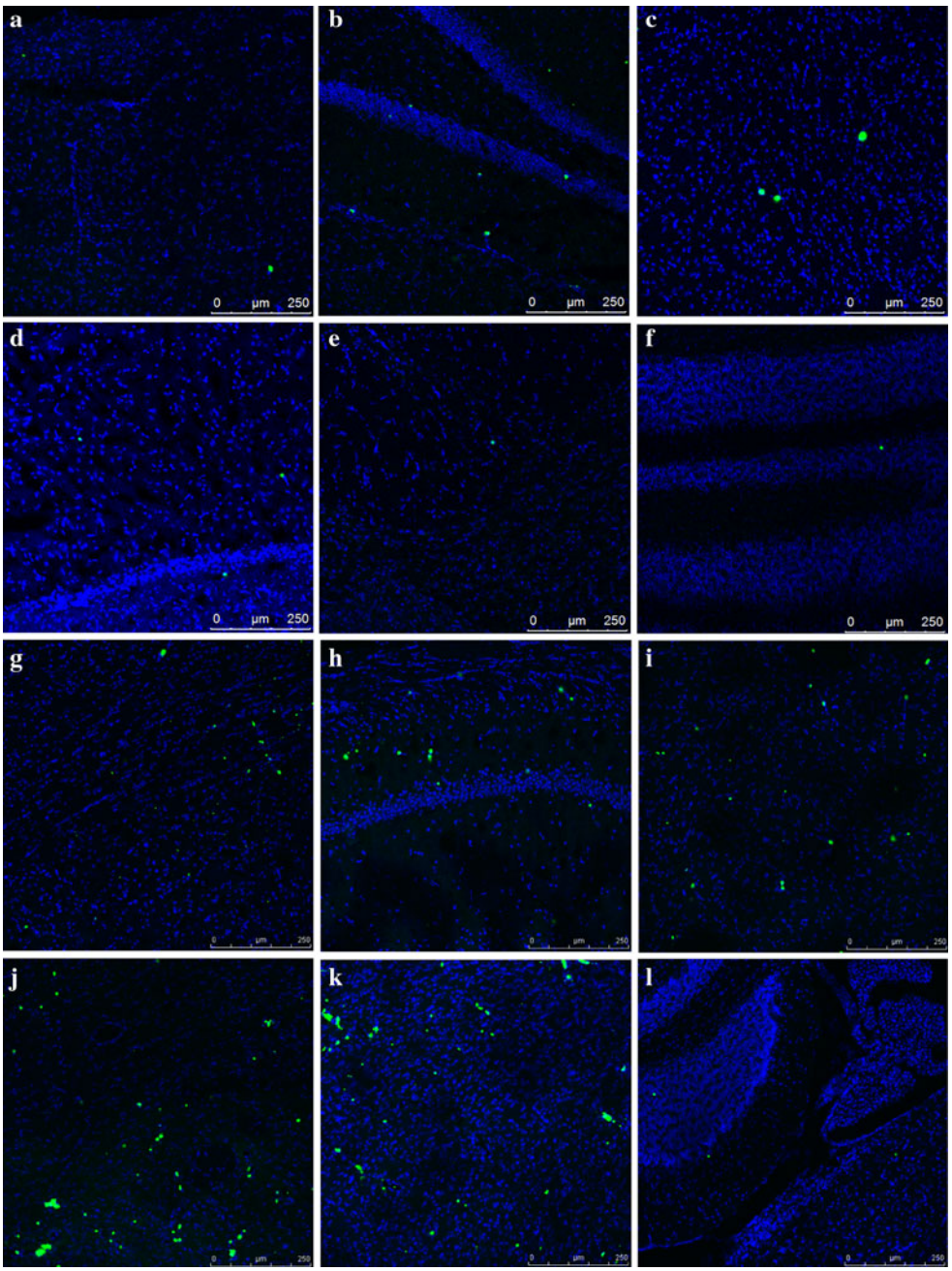

Fig. 6 The distribution of FMNs (**a**–**f**) and Tf-FMNs (**g**–**l**) in corpus striatum (**a**, **g**), hippocampus (**b**, **h**), thalamus (**c**, **i**), substantia nigra (**d**, **j**), mesencephalon (**e**, **k**), and cerebellum (**f**, **l**) (Color figure online)

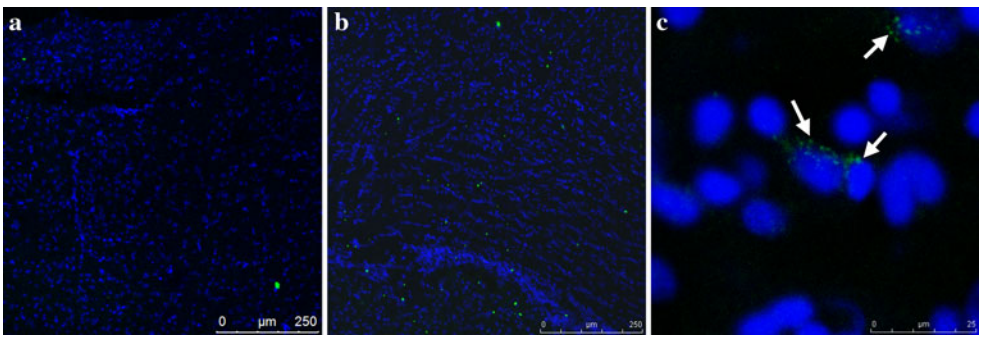

Fig. 7 The distribution of FMNs (**a**) and Tf-FMNs (**b**, **c**) in brain. *Scale bar* in **a** and **b** is 250 μm and *scale bar* in c is 25 μm. The *arrows* indicate the Tf-FMNs discretely distribute surrounding the nucleus stained by DAPI (Color figure online)

To determine BBB crossing ability of Tf-FMNs, the brain tissues were divided into six different regions (corpus striatum, hippocampus, thalamus, substantia nigra, mesencephalon and cerebellum). CLSM images obtained from these different regions are illustrated in Fig. 6. Both FMNs (Fig. 6a–f) and Tf-FMNs (Fig. 6g–l) were found in all six brain regions. However, the green fluorescence dots of FMNs (Fig. 7a) were weaker and aggregated, suggesting that most FMNs were still detained in the blood capillaries [19]. In contrast, the green fluorescence signals from Tf-FMNs were stronger (Fig. 7b) and discretely distribute surrounding the nucleus (Fig. 7c, as indicated by arrows), suggesting that Tf-FMNs indeed penetrated the BBB. Roberts et al. [20] characterized the endocytic pathway of Tf in BBB endothelial cells and concluded that Tf was taken up by receptor-mediated endocytosis at the luminal membrane of brain capillaries. The mechanisms of endocytosis were investigated in vitro by Visser et al. [6] and it

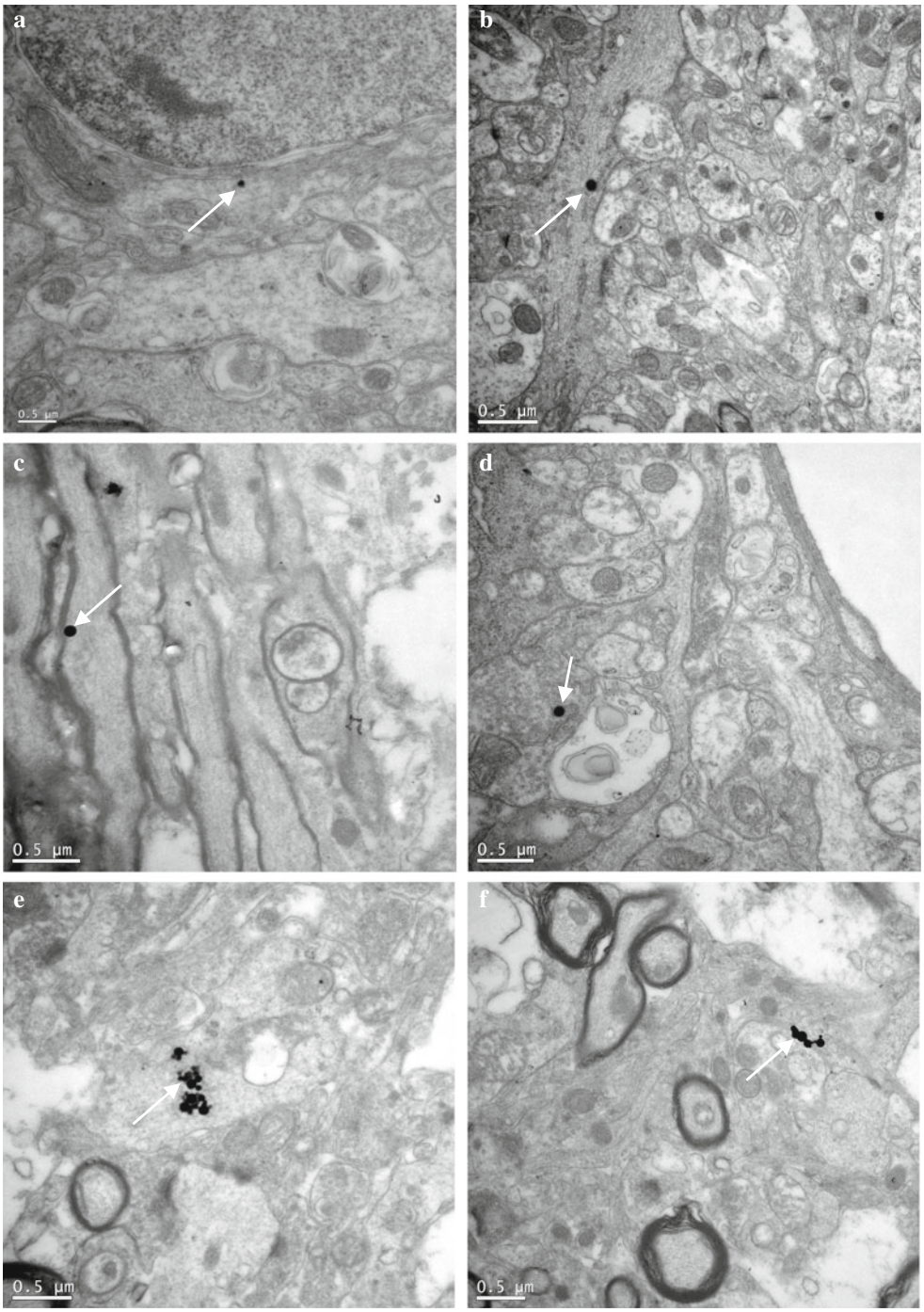

Fig. 8 TEM images of brain sections sacrificed 1 h post-injection with Tf-FMNs (as indicated by *arrow*), **a** in the cytoplasm of neuron, *scale bar* is 500 nm, **b** in the neurodendron of neuron, *scale bar* is 500 nm, **c** in the cylindraxile of neuron, *scale bar* is 500 nm, **d** in the synapse of neuron, *scale bar* is 200 nm, **e** in the process of brain cell, *scale bar* is 500 nm, **f** in the cytoplasm, *scale bar* is 500 nm

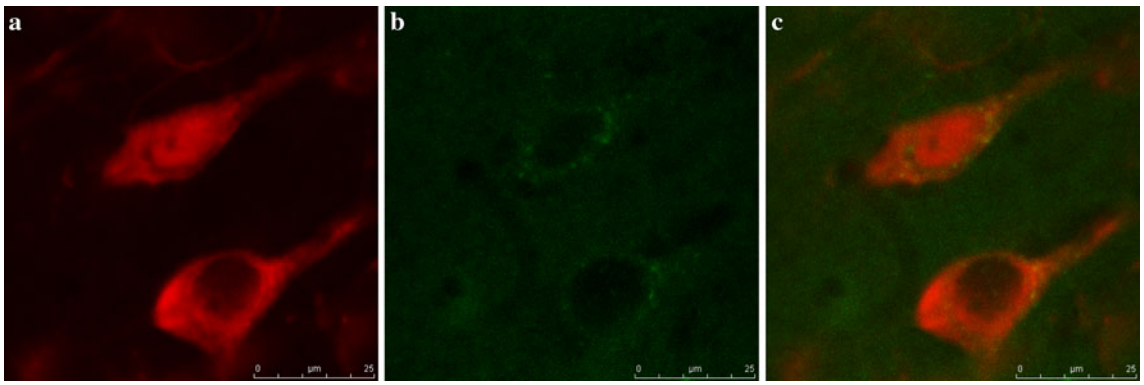

Fig. 9 CLSM images of brain sections sacrificed 1 h post-injection with Tf-FMNs. **a** neurons (*red*), **b** FITC-labelled nanoparticles (*green*), **c** merged micrographs of **a**, **b**. *Scale bar* is 25 μm (Color figure online)

was found that Tf was actively endocytosed by the Tf receptor on primary cultured bovine brain capillary endothelial cells in a concentration and time-dependent manner. Therefore, the enhanced BBB penetration ability of Tf-FMNs can be attributed to Tf conjugation, which facilitates the FMNs crossing the BBB by the receptor-mediated transcytosis [21].

Next, to identify the distribution of Tf-FMNs in brain cells, ultrathin sections of brains were examined at the subcellular level using TEM with high magnification. As shown in Fig. 8, Tf-FMNs were found not only in the cytoplasm and dendrite, but also in the axon and synapse of neurons that did not attach to the wall of the cerebral vessel (Fig. 8a–d). Since the BBB is located at the cerebral capillary endothelial cells which are connected by tight junctions, the uptake of Tf-FMNs by brain neurons indicated that these nanoparticles did penetrate the BBB and then entered the parenchyma. In contrast, FMNs were only observed inside the blood vessels (data not shown). However, it was noted that few number of Tf-FMNs in neurons was presented. This is because the nanoparticles would be diluted at least 200-fold after penetrating the BBB and this dilution effect may become even stronger after migrating to other brain cells [22].

To further verify that Tf-FMNs indeed diffused into neurons, immunofluorescence staining was performed to specifically label the neurons with anti-NeuN antibodies that recognize a neuron-specific antigen. CLSM was then utilized to inspect the colocalization of Tf-FMNs in neurons. The neurons were presented as red fluorescence signals due to the specific staining of anti-NeuN (Fig. 9a), while Tf-FMNs were shown as green fluorescence spots due to the FITC (Fig. 9b). The colocalization of red (neuron) and green (Tf-FMNs) resulted in yellow dots (Fig. 9c), clearly demonstrated that the presence of the Tf-FMNs in brain is due to the neuronal uptake.

The Tf-FMNs have been demonstrated to be able to cross the BBB. However, accumulation of the nanoparticles in the brain may result in neurotoxicity. Therefore, the brain sections from animals treated with Tf-FMNs were collected 24 h after the injection to primarily evaluate the biocompatibility. It was found that the green fluorescence almost disappeared or decreased remarkably (images not shown), suggesting that the Tf-FMNs were not likely to induce cumulative intoxication.

4 Conclusions

In sum, Tf as the brain targeting ligand was successfully conjugated to the FITC loaded magnetic nanoparticle in order to overcome the BBB. The BBB crossing ability of as-prepared Tf-FMNs was demonstrated in vivo. The CLSM study verified that Tf-FMNs could penetrate the intact BBB and diffuse into neurons and the TEM analyse further validated that Tf-FMNs indeed distributed in cytoplasm, dendrites, axons and synapses of neurons. In addition to the BBB crossing ability, Tf-FMNs maintain intrinsic functions of bare Fe_3O_4 and fluorescent mesoporous silica materials such as magnetic targeting, simultaneous magnetic resonance (MR) and fluorescence imaging, and controlled release of drugs. Therefore, the Tf-FMNs could be further developed as an effective multifunctional platform for brain-targeted theranostics.

Acknowledgments The authors thank the financial supports from Beijing Municipal Education Committee (KM20110025007), Beijing Municipal Foundation for the Talents (2011D005018000001), Natural Science Foundation of China (81271639), and the Funding Project for Academic Human Resources Development in Institutions of Higher Learning under the Jurisdiction of Beijing Municipality (PHR201007114).

References

1. Chomoucka J, Drbohlavova J, Huska D, Adam V, Kizek R, Hubalek J. Magnetic nanoparticles and targeted drug delivering. Pharmacol Res. 2010;62:144–9.

2. Kumar A, Jena PK, Behera S, Lockey RF, Mohapatra S, Mohapatra S. Multifunctional magnetic nanoparticles for targeted delivery. Nanomed Nanotechnol Biol Med. 2010;6:64–9.
3. Pardridge WM. Blood-brain barrier delivery. Drug Discov Today. 2007;12:54–61.
4. Abbott NJ, Patabendige AAK, Dolman DEM, Yusof SR, Begley DJ. Structure and function of the blood–brain barrier. Neurobiol Dis. 2009;37:13–25.
5. Li HY, Qian ZM. Transferrin/transferrin receptor-mediated drug delivery. Med Res Rev. 2002;22:225–50.
6. Visser CC, Stevanovic S, Voorwinden LH, Gaillard PJ, Crommelin DJA, Danhof M, de Boer AG. Validation of the transferrin receptor for drug targeting to brain capillary endothelial cells in vitro. J Drug Target. 2004;12:145–50.
7. Veiseh O, Sun C, Fang C, Bhattarai N, Gunn J, Kievit F, Du K, Pullar B, Lee D, Ellenbogen RG, Olson J, Zhang MQ. Specific targeting of brain tumors with an optical/magnetic resonance imaging nanoprobe across the blood–brain barrier. Cancer Res. 2009;69:6200–7.
8. Lu CW, Hung Y, Hsiao JK, Yao M, Chung TH, Lin YS, Wu SH, Hsu SC, Liu HM, Mou CY, Yang CS, Huang DM, Chen YC. Bifunctional magnetic silica nanoparticles for highly efficient human stem cell labeling. Nano Lett. 2007;7:149–54.
9. Lopez–Lopez MT, Duran JDG, Delgado A, Gonzalez-Caballero F. Stability and magnetic characterization of oleate-covered magnetite ferrofluids in different nonpolar carriers. J Colloid Interface Sci. 2005;291:144–51.
10. Tsai CP, Chen CY, Hung Y, Chang FH, Mou CY. Monoclonal antibody-functionalized mesoporous silica nanoparticles (MSN) for selective targeting breast cancer cells. J Mater Chem. 2009;19:5737–43.
11. Santra S, Yang H, Stanley JT, Holloway PH, Moudgil BM, Walter G, Mericle RA. Rapid and effective labeling of brain tissue using TAT-conjugated CdS: Mn/ZnS quantum dots. Chem Commun. 2005;25:3144–6.
12. Yang S, Chen D, Li N, Mei X, Qi X, Li H, Xu Q, Lu J. A facile preparation of targetable pH-sensitive polymeric nanocarriers with encapsulated magnetic nanoparticles for controlled drug release. J Mater Chem. 2012;22:25354–61.
13. Liu J, Wang B, Hartono SB, Liu T, Kantharidis P, Middelberg APJ, Lu GQ, He L, Qiao SZ. Magnetic silica spheres with large nanopores for nucleic acid adsorption and cellular uptake. Biomaterials. 2012;33:970–8.
14. Huang S, Li C, Cheng Z, Fan Y, Yang P, Zhang C, Yang K, Lin J. Magnetic Fe_3O_4@mesoporous silica composites for drug delivery and bioadsorption. J Colloid Interface Sci. 2012;376:312–21.
15. Knezevic NZ, Slowing II, Lin VSY. Tuning the release of anticancer drugs from magnetic iron oxide/mesoporous silica core/shell nanoparticles. ChemPlusChem. 2012;77:48–55.
16. Lin YS, Tseng CT, Hung Y, Chang C, Mou CY. Synthesis of hollow silica nanospheres with a microemulsion as the template. Chem Commun. 2009;3542–3544:3542–4.
17. De Palma R, Peeters S, Van Bael MJ, Van den Rul H, Bonroy K, Laureyn W, Mullens J, Borghs G, Maes G. Silane ligand exchange to make hydrophobic superparamagnetic nanoparticles water-dispersible. Chem Mater. 2007;19:1821–31.
18. van Schooneveld MM, Vucic E, Koole R, Zhou Y, Stocks J, Cormode DP, Tang CY, Gordon RE, Nicolay K, Meijerink A, Fayad ZA, Mulder WJM. Improved biocompatibility and pharmacokinetics of silica nanoparticles by means of a lipid coating: a multimodality investigation. Nano Lett. 2008;8:2517–25.
19. Costantino L, Gandolfi F, Tosi G, Rivasi F, Vandelli MA, Forni F. Peptide-derivatized biodegradable nanoparticles able to cross the blood–brain barrier. J Controlled Release. 2005;108:84–96.
20. Roberts RL, Fine RE, Sandra A. Receptor-mediated endocytosis of transferrin at the blood–brain barrier. J Cell Sci. 1993;104:521–32.
21. Beduneau A, Saulnier P, Benoit JP. Active targeting of brain tumors using nanocarriers. Biomaterials. 2007;28:4947–67.
22. Bickel U, Kang YS, Yoshikawa T, Pardridge WM. In-vivo demonstration of subcellular-localization of antitransferrin receptor monoclonal antibody-colloidal gold conjugate in brain capillary endothelium. J Histochem Cytochem. 1994;42:1493–7.